Available online at www.sciencedirect.com

ScienceDirect

Procedia Structural Integrity 68 (2025) 626–633

Structural Integrity Procedia

www.elsevier.com/locate/procedia

European Conference on Fracture 2024

The Effect of Build Strategy on the Residual Stress Distribution in Additively Manufactured Duplex Stainless Steel Pressure Vessels

A. E. Odermatt[a]*, N. Al-Hamdany[a], G. Abreu Faria[b], S. Degener[b], N. Kashaev[a]

[a]*Helmholtz-Zentrum Hereon, Institute of Material and Process Design, Max-Planck-Straße 1, 21502 Geesthacht, Germany*
[b]*Helmholtz-Zentrum Hereon, Institute of Material Physics, Max-Planck-Straße 1, 21502 Geesthacht, Germany*

Abstract

The resistance to service loads and defects of additively manufactured structures can be significantly reduced due to residual stresses induced by inhomogeneous cooling during the manufacturing process. For duplex stainless steels solution annealing at approx. 1050°C is the only industrially accepted stress relieve treatment. This is often accompanied by severe deformation due to the low creep resistance of the alloy at this temperature. For economic reasons the parts should be used in the as-built state, where the residual stress distribution needs to be considered. We determined the residual stress distribution of simplified pressure vessel geometries using high energy white beam X-ray radiation and the hole drilling method. As a result of this study, two building strategies were evaluated for their ability to produce a compressive residual stress state on the media facing side of the parts.

Keywords: Additive manufacturing; Duplex stainless steel; Residual stress; High energy X-Ray diffraction

1. Introduction

One use case for additively manufactured duplex stainless steel (DSS) parts being investigated is the utilization as hydrogen storage tanks (Odermatt et al. 2021). For mobile applications, the material needs to exhibit a combination

* Corresponding author. Tel.: +49 4152 87 2507.
E-mail address: anton.odermatt@hereon.de

10.1016/j.prostr.2025.06.107

of high specific strength, good resistance to hydrogen corrosion and a competitive price. DSSs possess some resistance to hydrogen corrosion and high strength due to their passive layer and mixture of bcc and fcc crystal structures. The storage in metal hydrides is attractive because they allow a high volumetric storage density. For the charging and discharging of the hydride, active temperature management is needed. The heat exchanger elements can be integrated into the tank geometry using additive manufacturing techniques. Hydrogen atoms – due to their small size – have a special affinity to diffuse into prestrained material, causing a deterioration of the mechanical properties (Örnek et al. 2018).

A common way of mitigating the formation of strain mismatch in additive manufacturing is preheating of the build plate, so that the temperature difference across the part during manufacturing is reduced. This approach is not recommended for DSSs (Schulze 2009; TMR Stainless 2014), as low interpass temperatures are needed to ensure high cooling rates for achieving the correct phase composition and impede the formation of intermetallic phases.

Stress relieve by annealing as a heat treatment is the most common way of diminishing residual stresses. For duplex stainless steel this is performed as a solution heat treatment at approx. 1050°C (Schulze 2009; TMR Stainless 2014) with subsequent quenching. Especially for large parts this is linked with high costs and the possibility of warping due to stress relief (Zinke 2021), creep (Schulze 2009) and uncontrolled inhomogeneous cooling. Residual stress design is therefore an essential component of the part design process with duplex stainless steels.

In additive manufactured parts, design parameters like the order of deposition sequences determine the residual stress state of the part. Newly deposited material solidifies, cools and contracts. The substrate or already deposited material is at a lower temperature than the deposited material. Due to the difference in temperature, the thermal shrinkage is inhomogeneous, resulting in strain mismatch and therefore residual stresses. These stresses reduce the useable load range of parts and therefore need to be considered in the design phase. Stress concentrations and their interaction with additional operational demands like wear and corrosion are of special interest. Designing the order of manufacture for tank structures for example, so that the media facing side is placed under compressive, or at least not tensile stresses might aide in improving the performance.

2. Methods

The approximate sample tank geometry investigated in this study is shown in Figure 1 (a). It has a square footprint (80 mm × 80 mm) with round corners (R=10 mm) and a height of approx. 80 mm. Rounding of the corners was performed to reduce stress concentrations and improve producibility. The measurement locations were chosen so that the expected residual stress field can be validated, and the expected maximum residual stresses can be determined.

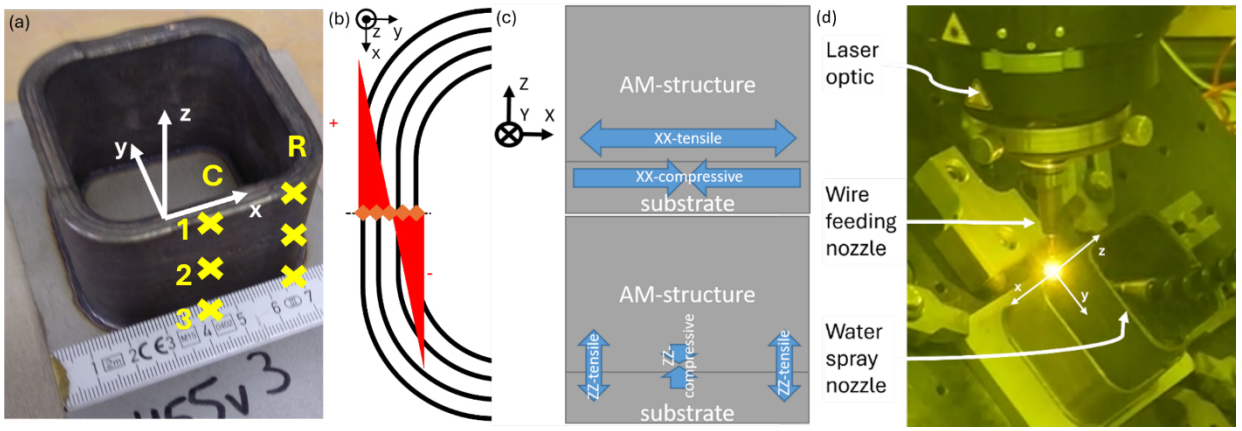

Figure 1 (a) Sample geometry with strain measurement locations, (b) expected residual stress distribution in a single layer, (c) global residual stress distribution in the whole part and (d) Cladding build strategy.

The first tank geometry was deposited using a layer wise build strategy: For every layer three tracks were deposited with the order from the inside to the outside of the sample. The height offset for every layer was 0.85 mm and the lateral offset between layers was 1.8 mm. A laser power of 2.5 kW and welding speed of 1 m/min were employed. The wire (3Dprint AM 2209 wire) feed rate was controlled to achieve a constant motor current, thereby stabilizing

the process. The inside track was deposited directly after the outside track of the preceding layer. For the center and outside tracks waiting times were implemented, so that the interpass temperature was kept below 300°C (measured with an Optris PI400 infrared camera).
For the second build strategy, the inside wall was deposited in one screw-like continuous deposition sequence using the same laser power and height offset per layer. The final wall thickness was obtained by two additional cladding passes using the same offset in the z-direction and lateral direction (Figure 1 (d)). The tool orientation was rotated 45° (Figure 1 (d)) around the weld track direction (x-direction in Figure 1 (a)) so that the bottom of sample, where substrate and additively manufactured part meet, could be cladded. To ensure high cooling rates during the continuous deposition the part was cooled with sprayed water from the inside during the deposition process.
The general expected stress distributions are shown in Figure 1 (b) and Figure 1 (c). During deposition of the cross section the outer layers contract, placing the inner layers under compressive stresses, while being kept in a tensile stress state. Viewed from a side, the contraction of the deposited material causes tensile stresses in the horizontal direction of the deposited material along the track direction, which are balanced by compressive stresses in the substrate. This stress distribution leads to an upward bending of the substrate, which is accompanied by tensile stresses in vertical direction in the edges of the part and compressive stresses in the center.
The process design was chosen, so that the austenite content is maximized at the inside of the wall to increase the corrosion resistance and the ferrite content is increased at the location of the outer tracks to achieve higher strength while still conforming to the requirements placed on wrought material and weld metal regarding the ferrite content (Schulze 2009).

2.1. Microstructural Characterization

The microstructure of the material was characterized using optical microscopy. Samples were cut from the tank structures using abrasive cutting. The samples were ground using emery paper and polished using diamond and aluminum oxide suspensions. Consequently, the samples were color etched using the Beraha II solution. Images were acquired on a Keyence VHX-7100 Microscope with a motorized stage at magnification of 400x in monochrome mode. For each sample a series of image from the bottom to the top of the structure were taken in the center of the inside, center and outside track respectively. The ferrite fraction of the material was determined automatically using Otsu's method (Otsu 1979).

2.2. Resdiual Stress Determination using High Energy X-Ray Diffraction

Polychromatic X-ray radiation was used for the measurement of residual strain in the additively manufactured tank structure produced with layer wise build strategy. The beamline P61A at DESY was chosen due to the high energy radiation, which allows measurements on materials with high absorptivity and thicknesses of multiple millimeters. The $sin^2\psi$-method was used to gather data and compute residual stresses. The data was analyzed using the P61Atoolkit (Gleb Dovzhenko 2021). The residual strain profiles were measured in two regions: At the middle of the sample and at the start of the radius section (Figure 1 (a)).
For each region the residual strain profiles through the wall thickness were measured in three positions (5mm from the bottom, in the middle (40 mm from the bottom) and 5 mm from the top surface of the additively manufactured structure (denoted as C1 to C3 (center) and R1 to R3 (radius)). For each of the six measurement positions 5 points were measured along the thickness direction of the sample. Wiggling in the plane of the walls of the sample with an amplitude of 5 mm in both directions (Y and Z) was employed to reduce the effects of the large grain size. The 2θ-angle was approx. 7.84°. Because the duplex microstructure is in different non-quilibrium states depending on the location in the sample, the chemical composition of austenite and ferrite, and thereby the stress-free lattice spacing (d_0) might vary. Therefore, the variation in the stress-free lattice spacing was measured on a second sample, where one weld track high stress-free lamella were cut by electrical discharge machining. For the d_0 sample measurements were made at three positions on the sample (5 mm, and 40 mm from the base and 5 mm from the top) and three points along the depth for each position resulting in nine measurements. For the calculation of the residual stresses, the values of d_0 were averaged over all positions because the expected variation was not seen in the data. Only the measurement data from the 211 peak for ferrite and the 311 peak for austenite were evaluated due to their low dependence on the texture of the material. The X-Ray elastic constants supplied with the P61A-Toolkit for bcc iron as well as

S_2 = -1.611×10^{-6} MPa and ½ S_2 = 6.94×10^{-6} for the fcc-phase (calculated with data from (Ledbetter 1985) using the Kröner model implemented in the XEC software by H. Wern (Wern et al. 1998)) were used to calculate the residual stresses.

2.3. Hole Drilling Method

The residual stresses were also determined by incremental hole-drilling method using PRISM system from Stresstech which is based on electronic speckle pattern interferometry. Further information about the working principle can be found elsewhere (Steinzig and Ponslet 2003). The measurement positions were the same as for the high energy X-ray diffraction. The measurement depth (1 mm) of the hole drilling method was limited to half the drill diameter (2 mm). Therefore, only the surface stresses at the outside of the samples could be determined. The residual stresses were calculated at twelve positions along the one-millimeter-deep measurement depth.

3. Results

3.1. Microstructural characterization

Optical measurements of the ferrite content yielded the ferrite fractions presented in Figure 2 (a) and Figure 3 (a) for the layer wise and cladding build strategy respectively. Because the interlayer waiting time was omitted for the deposition of the inside track during the layer wise build, the highest amounts of austenite were measured in this location. The bottom of the sample exhibits higher amounts of austenite. In this region, the epitaxial grain growth has not eliminated the grains which are not oriented in the fasted growth direction, yet. Therefore, there is an increased amount of ferrite/ferrite grain boundaries, from which austenite can precipitate. At the very top, increased amounts of ferrite are measured, because this region did not experience repeated reheating cycles.

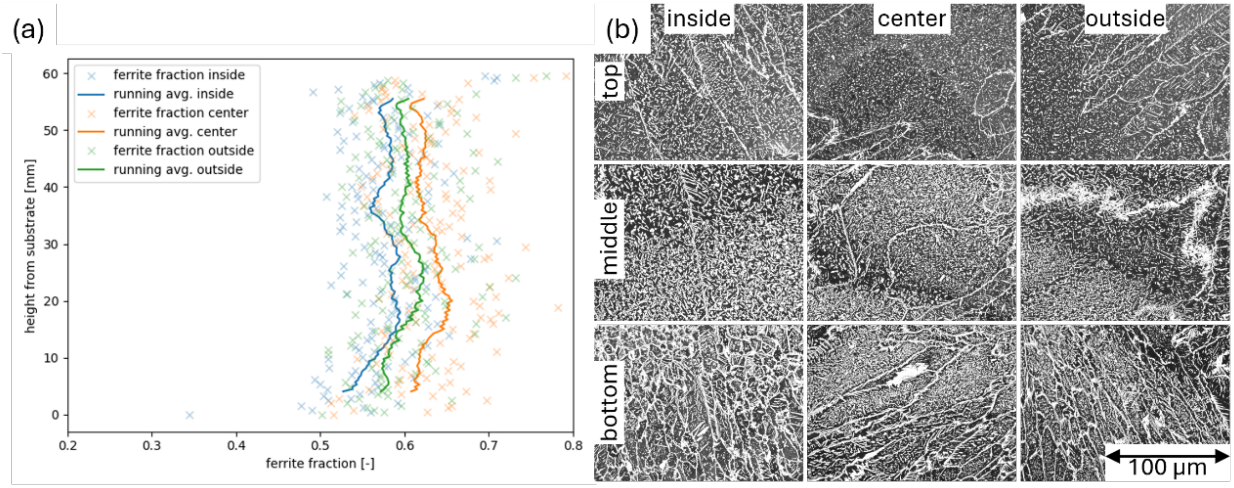

Figure 2: (a) Austenite-ferrite ratio in dependence of the weld track location and height of the sample for the layer wise build strategy. (b) Etched micrographs corresponding to the location (from left to right: top, center, bottom) and height of the sample (from top to bottom: approx. 60 mm, 30 mm, 1 mm).

The microstructure for the cladding build strategy (Figure 3) developed differently. The microstructure of the inside track is dominated by the epitaxial grain growth of the prior ferrite grains. The two cladded layers had two-dimensional heat transfer, whereby the epitaxial grain growth was inhibited. Due to the one-dimensional heat transfer in the inside tracks, lower cooling rates and thereby higher austenite contents were achieved. The cladded tracks exhibit higher ferrite contents due to the increased heat transfer. Also, the prior ferrite grain size is reduced due to the absence of epitaxial grain growth. This can also reduce the texture of the material.

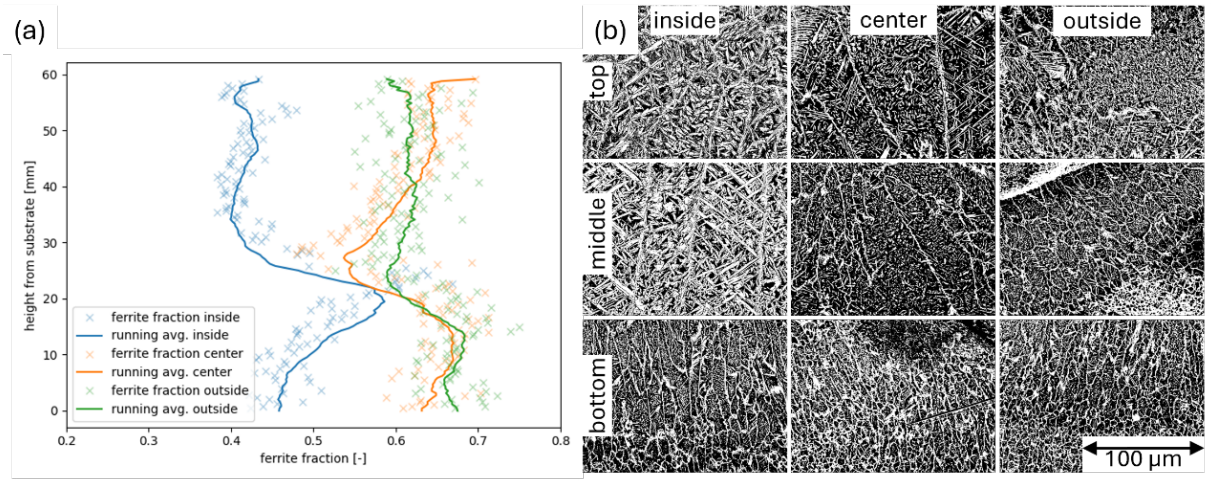

Figure 3: (a) Austenite-ferrite ratio in dependence of the weld track location and height of the sample for the cladding build strategy. (b) Etched micrographs corresponding to the location (from left to right: top, center, bottom) and height of the sample (from top to bottom: approx. 60 mm, 30 mm, 1 mm).

The results of the residual stress determination from the synchrotron measurements are shown in Figure 4. The results show that there are significant tensile stresses at the top of the sample in the weld track direction (C1 and R1, σ_{xx}). The stresses in track direction turn more compressive towards the bottom of the sample. At the corner of the sample the stresses are higher. In build direction (σ_{zz}) the stresses are more compressive in the center of the sample than on the corners. For the position C1 and R1 at the top of the sample, the stresses are nearly constant along the thickness of the wall. For C2, C3 and R3 the stresses are slightly more tensile towards the outside of the wall. For R2 the increase in stress is highest. The calculation of the residual stresses yielded results over the yield strength, but within the range of the ultimate tensile strength (Odermatt et al. 2022) of the material. The following factors influence the accuracy of the residual stresses significantly:

- accuracy of d_0
- accuracy of the x-ray elastic constants
- accuracy of the calculation of peak center energy in the scope of coarse grains and texture

Figure 5 shows the residual stresses determined using the incremental hole drilling method in more detail. Generally lower stresses (compressive stresses for the layer wise build strategy in the C1 and R1 location) were determined very close to the outside surface. The stresses increase until they reach a maximum between 0.25 mm and 0.5 mm depth and then decreases toward the bulk of the material. The main difference between the layer wise and the cladding build strategy is, that the latter produces significantly higher tensile residual stresses near the base of the sample. Consequently, the compressive residual stresses at the inside surface should be increased as well.

4. Discussion

The overall prediction from the process design could be confirmed. The calculated stresses qualitatively follow the expected trends. However significant tensile stresses are still present on the inside of some sections of the sample. The effect of the order of weld tracks has a lower effect than the order of layers. The effect for track order is reduced for increasing deposit height. The reason might be that succeeding tracks also have an influence on the stress distribution of preceding layers. Newly deposited material places all surrounding material, including the neighboring layer and the layers below, under compressive stresses while being placed under tensile stresses itself.

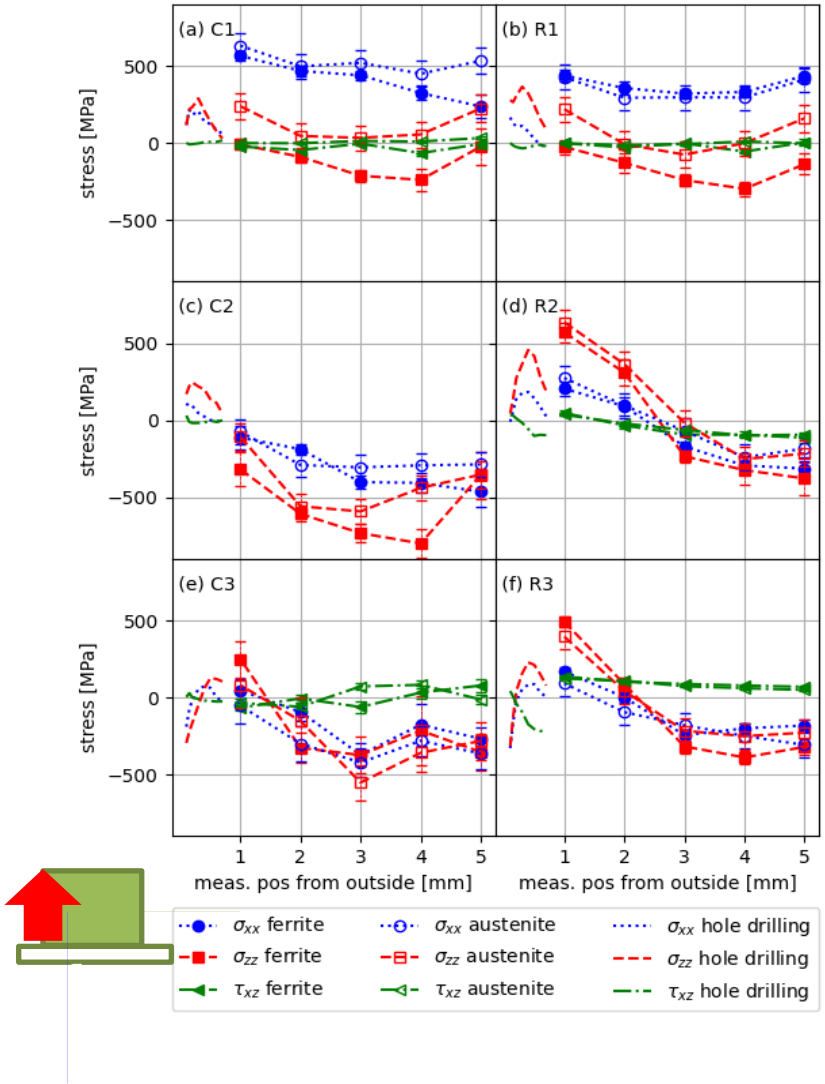

Figure 4: Residual stresses determined on the six positions of the additively manufactured sample.

Lu et al. (Lu et al. 2019) modelled the residual stress in additively manufactured rectangular hollow parts made from Ti-6Al-4V using the finite element method. They found the highest stresses (von Mises) in the transition area from substrate to additively manufactured parts. This is supported by the results of Ahmad et al. (Ahmad et al. 2018) who determined, that the highest residual tensile stresses are formed at the base of thin walled samples made via electron beam additive manufacturing. This is not supported by the results of this investigation, as it found compressive residual stresses in the corresponding (C3) location. Wu et al. (Wu et al. 2019) investigated the influence of the deposition pattern on the residual stress distribution in block-like wire arc additive manufactured Ti-6Al-4V and Inconel 718 using the finite element method. One of the deposition patterns was a spiral pattern where the material was deposited from outside to inside. They found high tensile stresses in the center of the component, where the deposition sequences ended and more compressive stresses on the outside. This follows the measured trends observed in this work regarding the deposition sequence. Lee et al. (Lee et al. 2019) investigated the effect of the tool path strategy on thin Ti-6Al-4V walls made with laser directed energy deposition with wire. They found a concentration of tensile residual stresses in build direction at the transition from the base plate to the deposited structure. The closest corresponding location in this work are the R3 and R2 positions, where tensile stresses can also be observed.

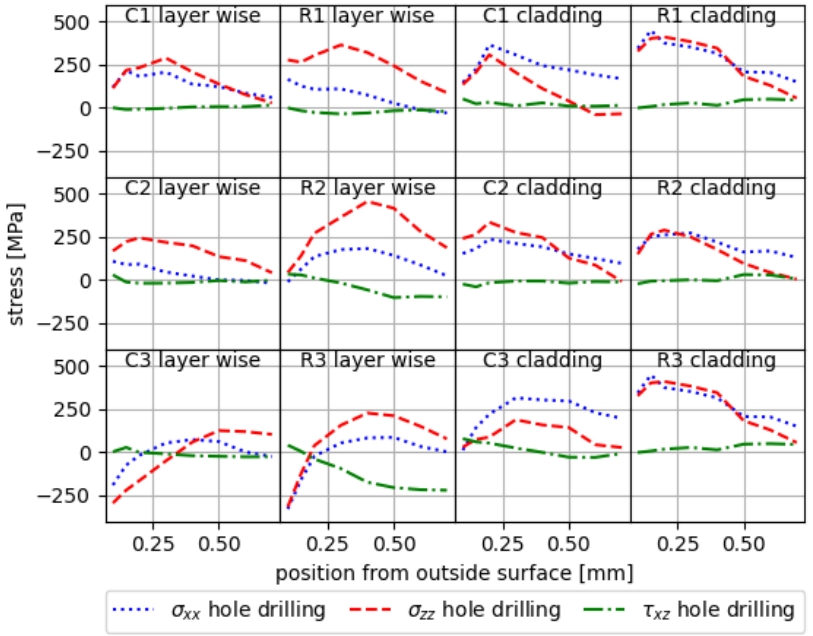

Figure 5: Residual stresses computed from relaxation strain using the incremental hole drilling method for the layer wise build strategy and cladding build strategies.

In summary, the objective of achieving only compressive residual stresses on the inside of the pressure vessel geometry could not be achieved using strategy 1. The severity of the residual stresses could be alleviated by the process design. The reason for this is, that the bending deformation from many successive layers in the build direction dominates over the contraction from the track order. Reversing the order of fabrication would have an adverse effect on the load bearing capacity of the pressure vessel. Using strategy 2 all measurement locations on the outside of the sample exhibited tensile stresses. Because tensile stresses need to be balanced by compressive stresses, we assume, that corresponding compressive stresses were generated on the inside of the sample using strategy 2. We conclude that the cladding build strategy is more beneficial regarding the residual stress state of the additively manufactured structure. However, the complexity of the manufacturing setup is higher, because at least 2 additional axes are needed to achieve the tilt of the part to be manufactured.

Acknowledgements

We would like to acknowledge the support of our colleague Falk Dorn in the laser materials processing department at the Institute of Material and Process Design for his support of our work.

References

Odermatt A., Passing M., J. Jepsen, T. Klassen, and N. Kashaev. 2021. Wasserstoffkorrosion mittels L-DED-wire gefertigter Duplexstähle. Wasserstoffeffekte in Werkstoffen, Exploratory Meeting of the DGM Group Hydrogen Effects in Materials.

Ahmad, B; van der Veen, Sjoerd O; Fitzpatrick, M. E; Guo, H. 2018. Measurement and modelling of residual stress in wire-feed additively manufactured titanium. Mater. Sci. Technol. 34, 18, 2250–2259.

Dovzhenko G., 2021. P61AToolkit. Helmholtz-Zentrum hereon GmbH, Geesthacht.

Ledbetter, H. M. 1985. Predicted monocrystal elastic constants of 304-type stainless steel. Physica B+C 128, 1, 1–4.

Lee, Y; Bandari, Y; Nandwana, P; Gibson, B. T; Richardson, B; Simunovic, S; Lee, Y; Bandari, Y; Nandwana, P; Gibson, B. T; Richardson, B; Simunovic, S. 2019. Effect of Interlayer Cooling Time, Constraint and Tool Path Strategy on Deformation of Large Components Made by Laser Metal Deposition with Wire. Appl. Sci. 9, 23, 5115.

Lu, X; Lin, X; Chiumenti, M; Cervera, M; Hu, Y; Ji, X; Ma, L; Yang, H; Huang, W. 2019. Residual stress and distortion of rectangular and S-shaped Ti-6Al-4V parts by Directed Energy Deposition. Modelling and experimental calibration. Addit. Manuf. 26, 166–179.

Odermatt, A. E; Dorn, F; Ventzke, V; Kashaev, N. 2022. Coaxial laser directed energy deposition with wire of thin-walled duplex stainless steel parts: Process discontinuities and their impact on the mechanical properties. CIRP J. Manuf. Sci. Technol. 37, 443–453.

Örnek, C; Reccagni, P; Kivisäkk, U; Bettini, E; Engelberg, D. L; Pan, J. 2018. Hydrogen embrittlement of super duplex stainless steel – Towards understanding the effects of microstructure and strain. Int. J. Hydrogen Energy 43, 27, 12543–12555.

Otsu, N. 1979. A Threshold Selection Method from Gray-Level Histograms. IEEE Trans. Syst., Man, Cybern. 9, 1, 62–66.

Schulze, G. 2009. Die Metallurgie des Schweißens. Eisenwerkstoffe, Nichteisenmetallische Werkstoffe. Springer-Verlag, s.l.

Steinzig, M; Ponslet, E. 2003. Residual Stress Measurement using the Holde Drilling Method and Laser Speckle Interferometry: Part 1. Exp. Tech. 27, 3, 43–46.

TMR Stainless. 2014. Practical Guidelines for the Fabrication of Duplex Stainless Steels, London, UK.

Wern, H; Johannes, R; Walz, H. 1998. Dependence of the X-Ray Elastic Constants on the Diffraction Plane. phys. stat. sol. (b) 206, 2, 545–557.

Wu, Q; Mukherjee, T; Liu, C; Lu, J; DebRoy, T. 2019. Residual stresses and distortion in the patterned printing of titanium and nickel alloys. Addit Manuf 29, 100808.

Zinke, M., 2021. Erzielung werkstoffspezifischer Eigenschaften beim generativen Schutzgasschweißen fertigkonturnaher Strukturen aus Duplexstahl. zu iGF-Vorhaben Nr. 20.361 BR. Schlussbericht vom 22.11.2021. Otto-von-Guericke-Universität Magedeburg Institut für Werkstoff und Fügetechnik, Magdeburg.